Diagnosing dry eye with dynamic-area high-speed videokeratoscopy

David Alonso-Caneiro
Jason Turuwhenua
D. Robert Iskander
Michael J. Collins

Diagnosing dry eye with dynamic-area high-speed videokeratoscopy

David Alonso-Caneiro,[a] **Jason Turuwhenua,**[b] **D. Robert Iskander,**[c] **and Michael J. Collins**[a]
[a]Queensland University of Technology, School of Optometry, Victoria Park Road, Kelvin Grove, QLD 4059 Brisbane, Australia
[b]Auckland Bioengineering Institute and the Department of Optometry and Vision Science, University of Auckland, Auckland, New Zealand
[c]Institute of Biomedical Engineering and Instrumentation, Plac Grunwaldzki 13, 50–377 Wroclaw, Poland

Abstract. Dry eye syndrome is one of the most commonly reported eye health conditions. Dynamic-area high-speed videokeratoscopy (DA-HSV) represents a promising alternative to the most invasive clinical methods for the assessment of the tear film surface quality (TFSQ), particularly as Placido-disk videokeratoscopy is both relatively inexpensive and widely used for corneal topography assessment. Hence, improving this technique to diagnose dry eye is of clinical significance and the aim of this work. First, a novel ray-tracing model is proposed that simulates the formation of a Placido image. This model shows the relationship between tear film topography changes and the obtained Placido image and serves as a benchmark for the assessment of indicators of the ring's regularity. Further, a novel block-feature TFSQ indicator is proposed for detecting dry eye from a series of DA-HSV measurements. The results of the new indicator evaluated on data from a retrospective clinical study, which contains 22 normal and 12 dry eyes, have shown a substantial improvement of the proposed technique to discriminate dry eye from normal tear film subjects. The best discrimination was obtained under suppressed blinking conditions. In conclusion, this work highlights the potential of the DA-HSV as a clinical tool to diagnose dry eye syndrome. © *2011 Society of Photo-Optical Instrumentation Engineers (SPIE).* [DOI: 10.1117/1.3598837]

Keywords: tear film; corneal topography noninvasive methods; ray-tracing; image analysis; biomedical optics; information processing.

Paper 11090R received Mar. 1, 2011; revised manuscript received May 18, 2011; accepted for publication May 19, 2011; published online Jul. 11, 2011.

1 Introduction

Dry eye syndrome is one of the most commonly reported eye health problems.[1] Current available methods to assess the tear film and to diagnose dry eye syndrome show some limitations to discriminate dry eyes from normal patients. Among them, traditional methods are, in most cases, invasive and have been criticized for their lack of repeatability or sensitivity.[2] Also, the agreement between some of the tests was found to be weak.[3] Various noninvasive tear film assessment methods have been investigated, but with limited discrimination performance.[4–9] Therefore, it is of clinical importance to improve the techniques for the assessment of tear film and the diagnosis of dry eye.

Noninvasive methods are defined here as methods in which no substance is instilled into the eye, there is no forced blinking or forcible holding of the eyelids, and there is no contact between the measuring instrument and the eye or eyelids. In the last decade, repeated measure videokeratography[4,10,11] and high-speed videokeratoscopy[12–14] (HSV) has emerged as one of the potential clinical tools to assess the tear film's integrity in a noninvasive manner.[12] Placido disk videokeratoscopy, which is the instrument investigated in this manuscript, is the current clinical standard for static measurement of corneal surface topography. In this technique, a set of concentric rings formed in a cone or bowl (i.e., the Placido disk) is projected onto the anterior surface of the eye and its reflection imaged on a camera [a charge-coupled device (CCD) type being the most popular among videokeratoscopes]. The reflection of the light is produced on the outer-most layer of the ocular surface, the tear film. Therefore, changes on the tear film surface induce changes in the structure and orientation of the reflected pattern. To maintain the optimal refractive power of the cornea, a regular and smooth tear film surface is required.[10,11]

Among the proposed techniques to assess tear film kinetics by means of videokeratoscopy, two different principles exist. Those that consider changes in corneal topography estimates[4,10,11,14] and those that consider changes in the structure of the reflected Placido disk image patterns.[13,15] Among the studies that focus on using topography information to assess tear film surface kinetics, different approaches can be identified. For example, height difference maps,[14] temporal changes in corneal power maps,[4] root mean square value of corneal aberrations,[10] and surface regularity and surface asymmetry indices[11] have been used as indicators of the tear film kinetics. However, the use of the topography information may not always produce desirable results. As previously noted,[13,16] the topography estimates provided by the instrument under strong Placido disk pattern disturbances may produce a topography map that is inaccurate (best case scenario) or not calculable at all (worst case). Also, some topography-based indicators (i.e., surface regularity indices or asymmetry indices) are highly sensitive to the ocular movements and misalignments[13] and may produce misleading results. To overcome these difficulties, progress has been made in devising image processing techniques that assess tear film integrity from a set of raw videokeratoscopy images (i.e., dynamic-area HSV) rather than using the instrument estimated topography information.[13,15]

In previous work, we extracted from each of the frames, composing the dynamic recording, a maximized area of analysis that is not affected by non tear disturbances[15] (i.e., shadows from eyelashes). Subsequently, an indicator of the pattern coherence (measurement of ring's orientation) called the tear film surface quality (TFSQ) indicator was determined.[15] Recent clinical studies using such an image processing-based technique to evaluate the TFSQ indicator have shown the potential of the dynamic-area HSV to assess the tear film under different circumstances, such as evaluation of the effects of soft contact lenses on the tear film,[12] for the assessment of normal tear film subjects[17] and for the diagnosis of dry eye.[18] In the current study, the evaluation of dry eye subjects and the discrimination from normal tear film subjects is further investigated. The effect of tear film surface kinetics (topography changes) on the Placido disk pattern is also presented. To achieve this goal, a ray-tracing model of the formation of a Placido disk pattern acquired from a given surface topography model is derived. Based on the observations from the modeling, a new purpose built TFSQ indicator is proposed. The objective of this indicator is to increase the sensitivity of the method to quantify changes of the reflected pattern.[15] To evaluate the performance of the proposed indicator, a comparison with a previously reported coherence-based TFSQ indicator[15] is provided, by using data from a retrospective clinical study[18] of dry eye and normal tear film subjects under the natural and suppressed blinking conditions.

2 Modeling the Formation of a Videokeratoscopy Image

In Placido disk videokeratography, a set of concentric rings in a cone or bowl is projected onto the tear film surface. The reflection of the rings is subsequently captured using a CCD camera, and then processed to yield corneal topography and/or associated metrics. Typically, we expect gross surface changes in the underlying cornea to induce distortions in the observed Placido disk pattern, but these distortions are constant over time. However, thickness changes in the overlying tear film will lead to changes in the observed distortion over time and is the concern of this work. The law of reflection[19] is sufficient to explain the geometrical distortion of the ring pattern in videokeratoscopy. Therefore, we will apply this principle to investigate the expected distortion in the Placido rings, due to a known "dimple" model of the tear film, which is introduced in Sec. 2.1.

Consider then Fig. 1, showing an estimated intersection point (S^*) on the tear film, with associated incident ($i = S^* - S_0$) and reflected rays ($r = d - S^*$) (here, S_0 and d represent the source and pinhole positions, respectively). The xy components of the following objective function:

$$e(S^*) = n^*(S^*) - n(S^*), \qquad (1)$$

will be the (2D) zero vector at the actual surface point, S, in accordance with the law of reflection. Here n^* is the normal to the estimated surface point $S^* = (x, y, f(x, y))$ and is given by

$$n^* = \left(\frac{\partial f}{\partial x}, \frac{\partial f}{\partial y}, -1 \right). \qquad (2)$$

The apparent normal to the surface n is the normal calculated by bisecting the incident, i, and reflected rays, r, by the following
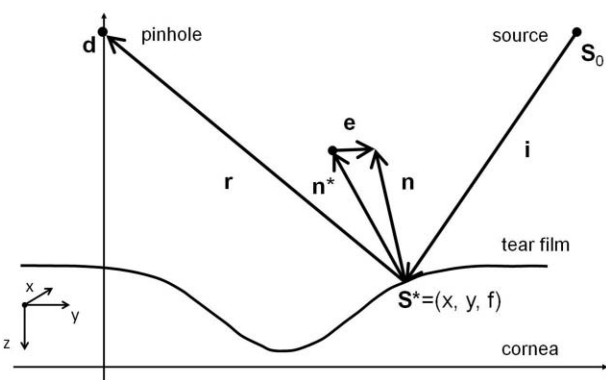

Fig. 1 Ray tracing model. The correct tear film position is determined by taking the difference of the surface and calculated normals. The required tear film position occurs when the difference is the zero vector.

rule:

$$n = \frac{\hat{r} - \hat{i}}{|\hat{r} - \hat{i}|_z}. \qquad (3)$$

This equation is normalized to have a negative but unitary z component [and so can be compared directly with Eq. (2)].

Having defined the problem, we use Powell's method[20] to iteratively locate the zero of Eq. (1) given a first estimate for the actual surface position, S. It is noted here, that situations where multiple reflections occurred were ignored and only single reflections were considered. To facilitate this outcome, a set of initial estimates was chosen over the cornea, allowing multiple local minima to be detected.

Once the tear film point S is determined, we can project the ray to the CCD plane (q) by a linear translation along the reflected ray,

$$q = \frac{r}{|r|_z} \Delta z + S, \qquad (4)$$

the subscript z indicates normalization by the absolute value of the z component only, and Δz is the horizontal distance from the tear film to CCD. The first two components of the q vector are xy positions on the CCD. The third component will be the axial position of the CCD and can be discarded.

2.1 Example: Tear Film Break-up Model

To simulate the effect of the topography changes on the reflected image during tear film break-up we assume a Gaussian tear film "dimple,"[21] based on fitting data from interferometry measurements of tear film topography,[22] added it to a spherical base (radius R) representing the cornea. The combined model is,

$$f(x, y) = a e^{-b\rho_0(x,y)^2} - \sqrt{R^2 - \rho(x, y)^2} + R.$$

Here a is the depth of the dimple, $b = -\ln(1/2)/(\rho_{hw}/2)^2$ is a constant related to the half width ρ_{hw}, while $\rho = \sqrt{x^2 + y^2}$ and $\rho_0 = \sqrt{(x - x_0)^2 + (y - y_0)^2}$ are radial distances from the corneal apex and dimple center (x_0, y_0), respectively.

We only need to perform ray-tracing using the section of the source ring involved in imaging the Gaussian dimple, as shown in Fig. 2. Hence, we delineate a region of interest on the cornea, and project that region back to a given source ring (with
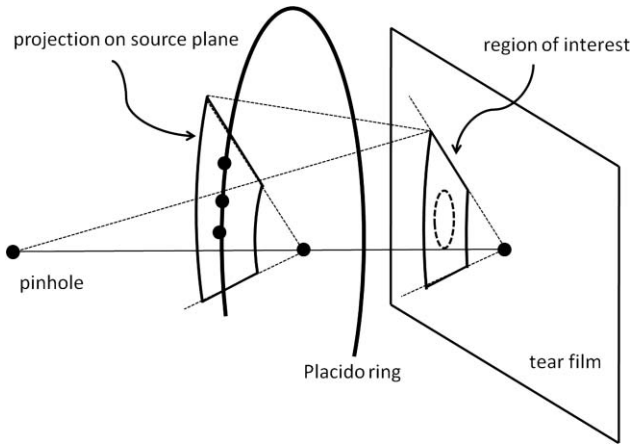
Fig. 2 Region around the Gaussian dimple is identified and then projected to the source plane. Only those parts of the source ring that fall within the projected area are ray-traced.

axial position z_s and radial extent r_s). The section of the ring that falls within the region of interest (on the source plane), can be discretized. Each discretized point is used to determine an intersection point using the optimization methods just described. The resulting set of S values can be projected to the CCD plane [Eq. (4)], yielding the predicted image of the dimpled region of the cornea.

Figure 3(a) shows a result of modeling assuming a dimple with values of $a = 0.001$ mm, $\rho_{hw} = 0.18$ mm, $x_0 = 1.4$ mm, and $y_0 = 0$ mm. The pinhole lies at $d = -30$ mm from the cornea along the optic axis, with CCD at $z = -60$ mm, and a source plane at $z_s = -10$ mm. The angle subtended by the source is $\pi/30$ radians about a horizontal axis. The source area contains 11 rings extending from $r_s = 6.2$ mm to $r_s = 7.5$ mm, that results in the region on the CCD shown. Figure 3(b) shows similar regions obtained from a real videokeratoscopy image. The simulation predicts significant distortion in the observed rings due to small amplitude changes in the tear film profile and the modeled images resemble those seen in actual tear film break-up images,[16,23] as shown in Fig. 3(b).
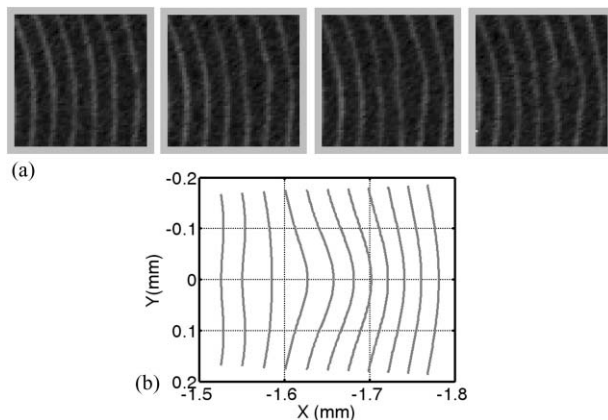

Fig. 3 (a) Sequence of four frames from a real section of a Placido disk image. (b) Predicted section of a Placido disk image at the CCD plane, as determined by the optimization method.

The proposed method does have certain limitations. While the possibility of multiple images is detected, the detailed handling of this situation was not investigated. Instead, our attention was restricted to shallow smoothly varying profiles where multiple images did not arise. Second, the model here does not include the potential scattering present near the center of a dimple. Nevertheless, for understanding tear film surface kinetics and mechanisms for early detection of tear film changes, the scatter should only become significant when the tear film break-up is well advanced.

2.2 Example: Simulated Effect on the Tear Film Surface Quality

Based on the Gaussian break-up model presented above, an example is provided here to assess the behavior of the previously proposed TFSQ indicator, which was based on the coherence (measurement of orientation) of the ring pattern.[15] The depth of the Gaussian dimple (a) is changed to simulate different stages of the tear film break-up. In this example, the Gaussian dimple's depth is varied between 1 μm and 5 μm, as this range of values corresponds to that of the tear film thickness.[24] From each dimple depth, a videokeratoscopy image is formed and the corresponding coherence-based TFSQ indicator is calculated. The normalized coherence-based TFSQ indicator is shown by a solid black line in Fig. 4. It is worth noting that the indicator presents a nonlinear response. Initially, it shows a slower decay until the depth of the break-up model reaches 3 μm, and after that a faster decay response is obtained. For early detection of changes it is desirable that the indicator presents a faster response in the initial stages. In an ideal case, the desirable indicator should quantify the changes of the topography model equally at all stages of tear break-up (i.e., having a linear response).

In Sec. 3, we have extended the current technique of dynamic-area high-speed videokeratoscopy (DA-HSV) by introducing a new TFSQ indicator, called the block-feature TFSQ indicator, which provides a faster response to the initial topographic changes by examining the rings variability in block sections across the image.

3 Block-feature Tear Film Surface Quality Indicator

The DA-HSV technique operates on a set of images that comprises the dynamic videokeratoscopy acquisition. Each videokeratoscopy gray-scale intensity digital image forms a 2D matrix $I(n, m)$, with $n = 1, 2 \ldots, N$ and $m = 1, 2 \ldots, M$. In the Medmont E300 videokeratoscope (Medmont Pty Ltd., Melbourne, Australia), which has been used in this study, the matrix is $N = 648$ by $M = 572$ pixels.

After acquiring the video sequence, the initial steps are to detect blinks and significant eye movements, which may produce blurred images. Once the inter-blink interval has been automatically identified, the area of analysis (AOA) is extracted from each of the images. The AOA marks an elliptical region to be used for the analysis, which does not contain shadows from eyelashes. The methodology for blink identification, eye movement detection, and AOA extraction is presented in detail in Ref. 15. Once the AOA is extracted, the TFSQ indicator (measure of pattern regularity) on this videokeratoscopy image region can be
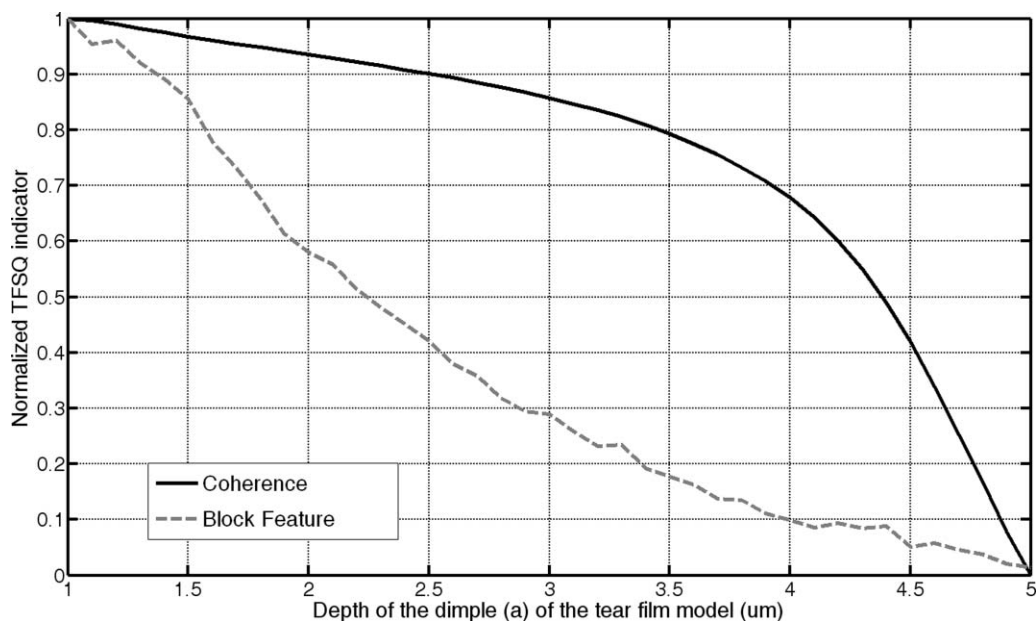
Fig. 4 Results of normalized TFSQ indicators for previous coherence-based[15] and current block-feature method, for different depth changes of the tear film break-up model.

calculated. Figure 5 summarizes the steps that are involved in the image processing procedure to extract the novel block-feature TFSQ indicator.

Once the original videokeratoscopy image is masked by the AOA, the image is transformed from Cartesian to polar coordinates. This step suppresses the influence of the Placido disk pattern's orientation on further image analysis by converting the circles into quasi-straight lines (in a specific direction). Similar conversion has been presented in Ref. 25. The Cartesian to polar transformation requires the location of the centroid of the innermost ring of the Placido disk image. If the instrument does not provide the centroid estimate, it could be calculated using geodesic morphological operators as has been presented in Ref. 23. We define a radial image profile as $I_p(r, \theta)$, where $r = 1, 2, \ldots, r_{max}$ and $\theta = 0, \delta_\theta, 2\delta_\theta, \ldots, 2\pi - \delta_\theta$, where δ_θ is a predetermined angular step. We can then form an $n_r \times n_\theta$ polar-grid matrix (image) with columns corresponding to sample radial profiles,

$$
I_p = \begin{bmatrix} I_p(1,0) & I_p(1,\delta_\theta) & \ldots & I_p(1, 2\pi - \delta_\theta) \\ I_p(2,0) & I_p(2,\delta_\theta) & \ldots & I_p(2, 2\pi - \delta_\theta) \\ \vdots & \vdots & \vdots & \vdots \\ I_p(r_{max},0) & I_p(r_{max},\delta_\theta) & \ldots & I_p(r_{max}, 2\pi - \delta_\theta) \end{bmatrix},
$$

where $n_r = r_{max} = 400$ and $n_\theta = 2\pi/\delta_\theta = 500$.[13] Figure 5(c) shows an example of the transformation.

The converted polar image, I_p, is divided into nonoverlapped blocks of equal size $W \times W$. The size of each block is chosen so it contains a significant number of rings without reducing the spatial resolution of the analysis. Taking into consideration the maximum width of a ring after the transformation, the block size has been empirically set to 26×26 pixels, which is sufficiently large to encompass up to three lines (polar domain). An image block centered at (n_b, m_b) is then defined as in Eq. (5), where

$$
n_b = \frac{W}{2}, \frac{W}{2} + W, \frac{W}{2} + 2W, \cdots, \frac{W}{2} + (\lfloor \frac{n_r}{W} \rfloor - 1)W
$$

and

$$
m_b = \frac{W}{2}, \frac{W}{2} + W, \frac{W}{2} + 2W, \cdots, \frac{W}{2} + (\lfloor \frac{m_\theta}{W} \rfloor - 1)W,
$$

with $\lfloor \cdot \rfloor$ denoting the floor operator.

A block-feature TFSQ indicator is calculated for each of the selected blocks $I_{block}[n_b, m_b]$. The idea underlying this indicator is to quantify the variability of the pattern over time, when the reflection from the tear film is specular (i.e., the tear film is smooth and regular) the pattern in the polar image has linear
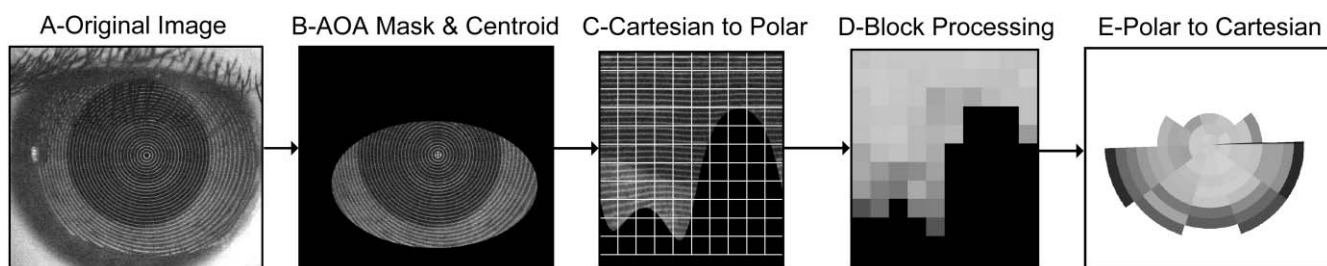

Fig. 5 Image processing steps to obtain the block-based tear film surface quality indicator.

orientation. As the reflection degrades, caused by irregularities of the tear film, the linear orientation of the pattern is compromised. Hence, by measuring the pattern's variation over time, an estimate of the TFSQ is obtained. The following steps are taken to extract the block-feature TFSQ indicator from each image block.

1. Normalization. A videokeratoscopy image is composed of two elements; the background (the anterior eye) and the foreground (the reflected pattern of the Placido disk rings). The anterior eye composing the background does not provide any essential information for the tear film analysis. Therefore, it is important to remove it from the image to avoid misleading information in further processing. This can be achieved with statistical block normalization, in which the block intensity information, $I_{block}[n_b, m_b]$, is normalized to zero mean and unit variance.[16]

$$I_{norblock}[n_b, m_b] = \frac{I_{block} - \hat{E}[I_{block}]}{\sigma[I_{block}]},$$

where $\hat{E}[\cdot]$ denotes the sample mean. It was empirically determined that when half or more of the values of the image block have been masked by the AOA, then the block is not taken into account

$$I_{block}(n_b, m_b) = \begin{bmatrix} \left[n_b - \frac{W}{2} + 1, m_b - \frac{W}{2} + 1\right] & \cdots & \left[n_b, m_b - \frac{W}{2} + 1\right] & \cdots & \left[n_b + \frac{W}{2}, m_b - \frac{W}{2} + 1\right] \\ \vdots & \ddots & \vdots & \ddots & \vdots \\ \left[n_b - \frac{W}{2} + 1, m_b\right] & & [n_b, m_b] & & \left[n_b + \frac{W}{2}, m_b\right] \\ \vdots & \ddots & \vdots & \ddots & \vdots \\ \left[n_b - \frac{W}{2} + 1, m_b + \frac{W}{2}\right] & & \left[n_b, m_b + \frac{W}{2}\right] & & \left[n_b + \frac{W}{2}, m_b + \frac{W}{2}\right] \end{bmatrix}. \quad (5)$$

2. Accumulation and peak detection. The block has the lines horizontally oriented, by accumulating the columns of the normalized block image, $I_{norblock}$, a vector, V, is obtained,

$$V(m_b) = \sum_{\alpha=1}^{m_b} I_{norblock}[n_b, \alpha].$$

V, which contains up to three peaks, is approximated by a sum of Gaussians[26] defined by,

$$f(x) = \sum_{j=1}^{3} A_j \exp\left[-\left((x - x_j)^2 / 2\sigma_j^2\right)\right].$$

Using a nonlinear least square algorithm, an estimate of the parameters to fit the data is obtained, $\hat{P}_f = [\hat{A}_j, \hat{x}_j, \hat{\sigma}_j]$, $j = 1, 2, 3$. The standard deviation from each of the Gaussian functions is extracted, $\hat{\sigma}_j$; these values provide an indication of the spread of the peaks. For example, quasi-straight lines lead to small standard deviations while if the line starts to degrade, due to tear film irregularities, the standard deviation increases.

3. Block-feature. The TFSQ indicator for the block is obtained as the average of the standard deviations of the extracted peaks, $\hat{G} = \hat{E}[\hat{\sigma}_1, \hat{\sigma}_2, \hat{\sigma}_3]$. To preserve the spatial information, a matrix of the same size as the polar image, $I_{BF}(n_r, n_\sigma)$, is created. Keeping the location of the block, all the values of the matrix that correspond to the evaluated block are set to the mean value of the standard deviation, $\hat{G}$.

Once the above three steps have been executed in each of the blocks [Fig. 5(d)], the spatial information of the image is recovered by converting the image back from polar to Cartesian coordinates, I_c [Fig. 5(e)].

The TFSQ indicator of the kth image has been defined as the profile sample mean within the AOA, where $TFSQ_k = \hat{E}[I_c]$. Unlike the coherence-based TFSQ indicator,[15] whose values are bounded between zero and one, this block-feature TFSQ does not have a bounded range. With the vector of average indicators given by,

$$TFSQ = [TFSQ_1, TFSQ_2, \ldots, TFSQ_K],$$

where K denotes the total number of frames that compose the video stream.

To assess the performance of the proposed block-feature TFSQ indicator, the same set of simulated videokeratoscopy images as presented in Sec. 2.2 is used. In this set, the sensitivity of the procedure to topography changes is observed. The normalized response of the proposed block-feature indicator is shown by a dotted gray line in Fig. 4. It is evident that it provides a faster response to the initial topography changes than the previously reported pattern coherence method.[15]

4 Clinical Study

4.1 Protocol

Data from a clinical study, reported in Ref. 18, is used here to evaluate the performance of the block-feature based dynamic-area HSV technique in the assessment of tear film surface quality of normal tear film subjects and subjects diagnosed with dry eyes

(i.e., poor tear film stability) under different blinking conditions. The retrospective data set was captured at 25 frames per second. Thirty four subjects participated in the study and were classified as dry eye or normal based on standard clinical assessments (i.e., battery of traditional invasive tests). According to this clinical classification, 22 normal subjects and 12 dry eye subjects participated in the experiment.

Two sets of measurements were carried out in the following order. In the first step, tear film surface quality was assessed in a suppressed blinking condition (SBC) and after a 10-minute break to ensure that the subject's tear film has recovered, again in natural blinking conditions (NBC). In the SBCs, three measurements were taken. Subjects were asked to blink several times before the beginning of the measurement and then focus on the instrument's fixation target and keep their eyes open as long as they could. The maximum time of the recording sequence was 30 s and a three-minute break was given between measurements. In the NBC experiment, the subject was asked to blink naturally without deliberately keeping their eyes open during two 30 s measurements. A break of 60 s was allowed for the subject before the next measurement was taken. After the acquisition, the dynamic-area HSV technique was used to obtain the AOA. For each inter-blink image of the recording, a value of TFSQ indicator was derived within the AOA using both image-processing techniques, based on the coherence[15] and the proposed block-feature algorithm.

The subject's data corresponding to a particular blinking condition was averaged across measurements and cropped to a specific length. The first second after the blink was excluded from the analysis to avoid the major effects of the tear film formation/spreading on the estimates of TFSQ values. After excluding the first second, in NBC only the first three seconds of inter-blink interval recording were considered while for the SBC, an 8 s recording was used. Receiver operating characteristics (ROC) curves, which determine the sensitivity and specificity of the measurement in diagnosing dry eye,[6] were calculated to show the capability of the two considered TFSQ indicators to discriminate dry eye from normal tear film subjects. To arrive at the best possible detection performance for the noninvasive test, a group of ROC curves were evaluated at different sampling intervals. This may provide a different time threshold for each of the blinking conditions (NBC and SBC) and the aim of this work was to evaluate the optimal time threshold in terms of discrimination performance.

4.2 Results

Figure 6 shows the ROC curves for the two considered TFSQ indicators (coherence versus block-feature) under different blinking conditions (NBC versus SBC). From each of the ROC curves, the area under the curve (AUC) was extracted using trapezoidal numerical integration (see legend in Fig. 6). AUC is bounded between zero and one, the closer to one the better the detector's performance.

Although AUC is one of the main parameters of ROC, to better evaluate the performance of the technique as a detector, (i.e., the discrimination between dry eyes from those of normal subjects) it is important to determine the so-called cut-off point, selected as the one that optimizes both sensitivity and specificity. Sensitivity measures the proportion of actual positives (i.e., dry
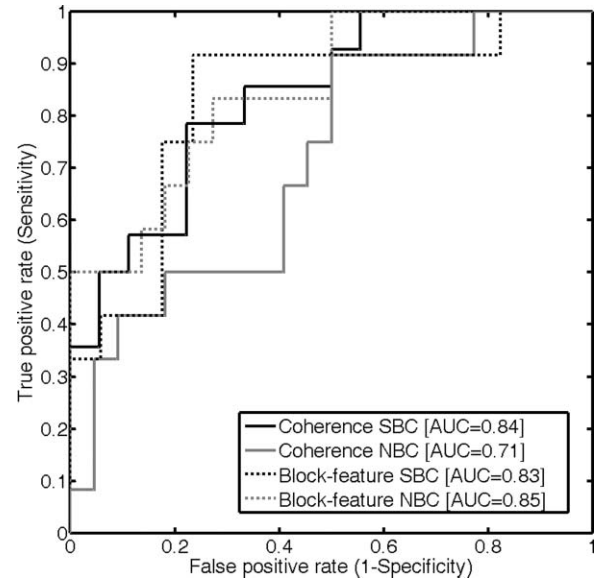

Fig. 6 Discrimination of dry eye subjects by dynamic-area high speed videokeratoscopy in both NBC and SBC.

eye subjects) that are correctly identified, while specificity measures the proportion of actual negatives (i.e., normal tear film subjects) that are correctly identified.

Table 1 shows a summary of sensitivity, specificity, and overall accuracy for each of the conditions, after the selection of the optimized cut-off point. To facilitate the detector performance's comparison, we evaluated every tested condition by means of a set of statistical tools,[27] namely the Youden's index (γ) and the discriminant power (DP). Youden's index evaluates the algorithm's ability to avoid failure and follows the expression

$$\gamma = sensitivity + specificity - 1.$$

The closer γ is to one, the better the performance. Equally, the discriminant power (DP) is a measurement that summarizes sensitivity and specificity of the technique,

$$DP = \frac{\sqrt{3}}{\pi} \left(\log X + \log Y \right),$$

where $X = sensitivity / (1 - sensitivity)$ and $Y = specificity / (1 - specificity)$. Values of $DP < 1$ indicate poor discrimination performance, $DP < 2$ indicates limited

Table 1 Test effectiveness of two different TFSQ indicators under different blinking conditions (BC). Sensitivity (Sens.), specificity (Spec.), overall accuracy (OA), Youden's index (γ), and discriminant power (DP). Suppressed blinking conditions (SBC) and natural blinking conditions (NBC).

TFSQ indicator	BC	Sens.	Spec.	OA	γ	DP
Coherence	SBC	0.79	0.72	0.75	0.51	1.24
	NBC	0.92	0.46	0.62	0.37	1.22
Block-feature	SBC	0.92	0.71	0.79	0.62	1.81
	NBC	0.83	0.68	0.74	0.52	1.31

performance, $DP < 3$ are considered to be a fair discrimination, while values above three are classified as good.

Based on the results from Table 1, the benefits in terms of the discrimination performance of the proposed block-feature technique is evident. Where the AUC does not show much difference, calculating Youden's index and the DP gives clearer evidence of the improvement in terms of the detector performance. The best results are obtained for the block-feature TFSQ indicator under suppressed blinking conditions.

5 Summary and Discussion

In this paper, the relationship between tear film topography changes and the obtained videokeratoscopy images have been investigated. By introducing a Gaussian model of the tear film break-up and the subsequent ray-trace procedure, changes in the videokeratoscopy images have been modeled. Although it is known that the tear film can adopt multiple shapes and different dimensions,[28] the Gaussian-based model used in this paper was similar to the one used in a study of interferometry topographic measurements.[21] By changing the characteristics of the Gaussian function, similar shapes to those reported in Ref. 28 could be replicated. Also, this representative model leads to a better understanding of the instrument's capabilities and limitations. It also sets a benchmark for the development of pattern orientation TFSQ indicators for tear film assessment, which with the help of this model, can be tuned to the specific topographic changes.

Based on the observations from the model, a novel indicator to assess the quality of the tear film surface has been proposed. This TFSQ indicator has shown good performance to discriminate dry eye from normal tear film subjects and it performs similarly to other well established methods based on different principles, such as osmolarity[29] or tear turnover rate.[6] Also, our technique provides similar results to those reported by Mengher et al.[8] who used a subjective assessment of the reflected Placido pattern to obtain tear film break-up time. The limited discrimination performance of any single method highlights the complexity of diagnosing dry eye syndrome. Normal tear film dynamics require adequate tear production, stability on the ocular surface and balanced elimination of the tears.[29] Quantitative or qualitative changes in any of these steps would imbalance the normal dynamics of the tears and may lead to dry eye syndrome. Hence, a range of different mechanisms could cause dry eye syndrome. As each instrument or technique assesses a different aspect of the tear film (e.g., dynamic-area HSV provides a measurement of the surface kinetics), it is unlikely that a single test would achieve very high discrimination power in the diagnosis of the dry eye syndrome.[6] Therefore, a combination of different tests may improve the efficacy of diagnosis. As such, the results of this study suggest that the dynamic-area HSV is a suitable test to be incorporated in the noninvasive diagnostic assessment of dry eye.

References

1. K. Tsubota, "Tear dynamics and dry eye," *Prog. Retin. Eye Res.* **17**(4), 565–596 (1998).
2. K. K. Nichols, G. L. Mitchell, and K. Zadnik, "The repeatability of clinical measurements of dry eye," *Cornea* **23**(3), 272–285 (2004).
3. T. A. Saleh, B. McDermott, A. K. Bates, and P. Ewings, "Phenol red thread test vs Schirmer's test: a comparative study," *Eye* **20**(8), 913–915 (2005).
4. T. Goto, X. Zheng, S. D. Klyce, H. Kataoka, T. Uno, M. Karon, Y. Tatematsu, T. Bessyo, K. Tsubota, and Y. Ohashi, "A new method for tear film stability analysis using videokeratography," *Am. J. Ophthalmol.* **135**(5), 607–612 (2003).
5. T. Goto, X. Zheng, S. Okamoto, and Y. Ohashi, "Tear film stability analysis system: introducing a new application for videokeratography," *Cornea* **23**(8), S65–S70 (2004).
6. S. Khanal, A. Tomlinson, A. McFadyen, C. Diaper, and K. Ramaesh, "Dry eye diagnosis," *Invest. Ophthalmol. Visual Sci.* **49**(4), 1407–1414 (2008).
7. J. C. Mainstone, A. S. Bruce, and T. R. Golding, "Tear meniscus measurement in the diagnosis of dry eye," *Curr. Eye Res.* **15**(6), 653–661 (1996).
8. L. S. Mengher, A. J. Bron, S. R. Tonge, and D. J. Gilbert, "A non-invasive instrument for clinical assessment of the pre-corneal tear film stability," *Curr. Eye Res.* **4**(1), 1–7 (1985).
9. C. Vitali, H. M. Moutsopoulos, and S. Bombardieri, "The European community study group on diagnostic criteria for Sjogren's syndrome. Sensitivity and specificity of tests for ocular and oral involvement in Sjogren's syndrome," *Br. Med. J.* **53**(10), 637–647 (1994).
10. R. Montes-Mico, J. L. Alio, G. Munoz, and W. N. Charman, "Temporal changes in optical quality of air-tear film interface at anterior cornea after blink," *Invest. Ophthalmol. Visual Sci* **45**(6), 1752–1757 (2004).
11. J. Nemeth, B. Erdelyi, B. Csakany, P. Gaspar, A. Soumelidis, F. Kahlesz, and Z. Lang, "High-speed videotopographic measurement of tear film build-up time," *Invest. Ophthalmol. Visual Sci.* **43**(6), 1783–1790 (2002).
12. D. Alonso-Caneiro, D. R. Iskander, and M. J. Collins, "Tear film surface quality with soft contact lenses using dynamic-area high-speed videokeratoscopy," *Eye & Contact Lens* **35**(5), 227–231 (2009).
13. D. R. Iskander, M. J. Collins, and B. A. Davis, "Evaluating tear film stability in the human eye with high-speed videokeratoscopy," *IEEE Trans. Biomed. Eng.* **52**(11), 1939–1949 (2005).
14. M. Zhu, M. J. Collins, and D. R. Iskander, "Dynamics of ocular surface topography," *Eye* **21**(5), 624–632 (2006).
15. D. Alonso-Caneiro, D. R. Iskander, and M. J. Collins, "Assessment of tear film surface quality using dynamic-area high-speed videokeratoscopy," *IEEE Trans. Biomed. Eng.* **56**(5), 1473–1481 (2009).
16. D. Alonso-Caneiro, D. R. Iskander, and M. J. Collins, "Estimating corneal surface topography in videokeratoscopy in the presence of strong signal interference," *IEEE Trans. Biomed. Eng.* **55**(10), 2381–2387 (2008).
17. D. H. Szczesna, D. Alonso-Caneiro, D. R. Iskander, S. A. Read, and M. J. Collins, "Lateral shearing interferometry, dynamic wavefront sensing, and high-speed videokeratoscopy for noninvasive assessment of tear film surface characteristics: a comparative study," *J. Biomed. Opt.* **15**(3), 037005 (2010).
18. D. H. Szczesna, D. Alonso-Caneiro, D. R. Iskander, S. A. Read, and M. Collins, "Predicting dry eye using non-invasive techniques of tear film surface assessment," *Invest. Ophthalmol. Visual Sci* **52**(2), 751–756 (2011).
19. S. A. Klein, "Corneal topography reconstruction algorithm that avoids the skew ray ambiguity and the skew ray error," *Optom. Vision Sci.* **74**(11), 945–962 (1997).
20. W. H. Press, *Numerical Recipes: the Art of Scientific Computing*, pp. 1235, Cambridge Univ Press (2007).
21. H. Kasprzak, "Modeling of the influence of the tear film deterioration on the cornea-on the refractive properties of the eye," *Mopane2003* **1**(1), 197–200 (2003).
22. T. J. Licznerski, H. T. Kasprzak, and W. Kowalik, "Application of Twyman–Green interferometer for evaluation of in vivo breakup characteristic of the human tear film," *J. Biomed. Opt.* **4**(1), 176–182 (1999).
23. W. Alkhaldi, D. R. Iskander, A. M. Zoubir, and M. J. Collins, "Enhancing the standard operating range of a placido disk videokeratoscope for corneal surface estimation," *IEEE Trans. Biomed. Eng.* **56**(3), 800–809 (2009).
24. E. King-Smith, B. Fink, R. Hill, K. Koelling, and J. Tiffany, "The thickness of the tear film," *Curr. Eye Res.* **29**(4), 357–368 (2004).

25. D. R. Iskander and M. J. Collins, "Applications of high-speed videok-eratoscopy," *Clin. Exp. Optom.* **88**(4), 223–231 (2005).
26. A. Goshtasby and W. D. O'Neill, "Curve fitting by a sum of Gaussians," *Graph. Models Image Process.* **56**(4), 281–288 (1994).
27. M. Sokolova, N. Japkowicz, and S. Szpakowicz, "Beyond accuracy, f-score and roc: a family of discriminant measures for performance evaluation," *AI 2006: Advances in Artificial Intelligence* **4304**(1), 1015–1021 (2006).
28. E. Bitton and J. V. Lovasik, "Longitudinal analysis of precorneal tear film rupture patterns," *Lacrimal Gland, Tear Film, and Dry Eye Syndromes 2: Basic Science and Clinical Relevance* **438**(1), 381–389 (1998).
29. A. Tomlinson, S. Khanal, K. Ramaesh, C. Diaper, and A. Mc-Fadyen, "Tear film osmolarity: determination of a referent for dry eye diagnosis," *Invest. Ophthalmol. Visual Sci* **47**(10), 4309–4315 (2006).